Authors' Accepted Manuscript of paper published in Polymers & Polymer Composites, Vol. 25, part 5, pp. 315-332 (2017); *Copyright Smithers Information Ltd.*

Synthesis and characterisation of novel thiophene based azomethine polymers and study of their liquid crystalline, electrochemical and optoelectronic properties

Omer Yasin Al-Janabi [a], Peter J. S. Foot* [b], Emaad Taha Al-Tikrity [a], Peter Spearman[b]

[a] Faculty of Science, Chemistry Department, Tikrit University Iraq

[b] Materials Research Centre and School of Life Science, Pharmacy & Chemistry, SEC Faculty, Kingston University London, Penrhyn Road, Kingston upon Thames KT1 2EE.

SUMMARY

This work reports the synthesis, structural characterisation, liquid crystallinity, luminescence and electroluminescence of novel thiophene azomethine polymers. The polymers under study were prepared via oxidative polymerisation of four novel monomers at room temperature using iron (III) chloride. The chemical structures of the prepared monomers and polymers were confirmed by infrared and ^{1}H and ^{13}C NMR spectroscopy. Molecular masses were determined for monomers and polymers by gas/liquid chromatography-mass spectrometry (GC/LC-MS) and by gel-permeation (size exclusion) chromatography (SEC), respectively. Thermal stability studies of the prepared materials were achieved by thermogravimetric analysis (TGA), and the onset of weight loss T_o and the endset T_{max} were calculated from the thermograms. Liquid crystalline mesophases and phase changes of the monomers and polymers were studied by differential scanning calorimetry (DSC) and polarised optical microscopy (POM), and the glass transition temperatures Tg of the polymers were determined from the DSC curves. The electrochemical band gaps, HOMO and LUMO energy levels were measured by cyclic voltammetry. UV-visible absorption-emission spectra (liquid and solid films) of the polymers were obtained at room temperature with different solvents. Optical band gaps were calculated from the absorption edges, and were in good agreement with those estimated from cyclic voltammetry. Mixing the polymers with lanthanide salts such as $EuCl_3$ and $YbCl_3$ gave sensitised fluorescence, and the light emitted was much more intense than that from the pure polymers. Polymer based light-emitting diodes (PLEDs) were fabricated by spin coating, and their current-voltage characteristics were measured. In preliminary work, the polymer devices were found to produce electroluminescent spectra similar to the PL spectra of the corresponding samples. Molecular modelling studies were performed on both polymer segments and monomer molecules; the absorption spectra of the prepared polymers, HOMO and LUMO energy levels were calculated with ZINDO using AMI geometry optimisation.

Keywords: Conducting polymer, thiophene, azomethine, liquid crystal, electroluminescence

* Corresponding author: p.j.foot@kingston.ac.uk

1. INTRODUCTION

Polyazomethine or Schiff-base polymers are interesting alternatives for to the luminescent polymer, poly(p-phenylenevinylene) (PPV), having CH=N linkages in the main chain that are comparable to C=C in PPV, and being capable of protonation and complexation with metal cations[1,2].

Aromatic polyazomethines are of particular interest owing to their good thermal stability, mechanical strength, nonlinear optical properties, semiconducting properties, environmental stability and fibre-forming properties. They may also be applicable in the field of polymer electronics, especially in view of the recent discovery that the photoluminescence of the conjugated polymers containing basic sites in the main chain could be modified by protonic (acid-base) doping[3]. Recent papers of Lehn *et al.* extend the polyazomethines study to the design of constitutional dynamic polymers, which are opening new perspectives in materials science, being a very powerful alternative to nanofabrication and nanomanipulation for the development of nanotechnology[4,5].

From a practical point of view, it is interesting to obtain functional azomethine polymers incorporating new properties such as luminescence and liquid crystallinity. The production of -CH=N- linkages does not require stringent reaction conditions[6]; given the synthetic advantages of azomethines and their expected similar properties to their vinyl cousins, it is important to assess their suitability for replacing functional materials currently used in organic electronic devices. Due to the twisted conformation around the aryl azomethine bonds which limits their degree of conjugation, their optoelectronic properties are not entirely comparable to their vinylene analogues. However, protonation or complexation of azomethine linkages can enhance their planarity and influence optoelectronic (photo- and electroluminescence) properties[2]. Another strategy to improve the π electron delocalisation along polyazomethine chains is to replace one of the phenylene rings with a heterocyclic ring such as a thiophene derivative[7-10]. This is partly due to the coplanarity of thiophene-azomethine moieties, resulting in extended delocalisation relative to the homoaryl azomethine.

There are some reported data about luminescent polyazomethines containing chromophoric units such as fluorene, triphenylamine, pyrene or thiophene side chains[2], but to the best of our knowledge, there are no previous reports examining the preparation and structure-property relationships of azomethines or polyazomethines consisting of a thiophene amine with a nitrile group at position 3 of the thiophene ring and aromatic aldehydes bearing liquid crystalline moieties in their side- or main-chain.

We were interested in investigating the effects of thiophene Schiff-base polymers containing electron-withdrawing cyano groups in position 3 of the thiophene ring on the photophysical and electrochemical properties of the polymers. Introduction of acceptor groups at the 3-position of the thiophene unit increases their oxidation potential. Roncali *et al* showed that the introduction of a cyano group at the vinylene linkage (of a dithienylene unit) could lead to a considerable reduction of the bandgap of the corresponding polymers. Another important point is that the cyano groups induce a decrease in the HOMO level, and thus a stabilisation of the neutral state of the polymers. In particular the modification of the electronic states, i.e. the bandgap and the positions of the HOMO and LUMO levels, enables useful control of the device engineering in photophysical applications such as photovoltaic diodes and electroluminescence.

In this work, we emphasise the design of novel functional thiophene polymers containing azomethine linkages in the main backbone and liquid crystalline moieties in the main chain and side chain of the polymer. Thiophene-2-amino-3-carbonitrile was chosen as the chromophoric unit and basis for the synthesis of four new thiophene Schiff-base monomers *via* reaction with four different aromatic dialdehydes. These were subsequently polymerised by chemical oxidation using iron (III) chloride. 2-aminothiophene-3-carbonitrile precursor is preferred instead of 2-aminothiophene because of the instability of the latter and the electron-withdrawing cyano group of the former, which would emphasise the electron-delocalising power of the thiophene unit.
Aromatic dialdehydes linked together with 2-aminothiophene-3-carbonitrile lead to an enhancement of the optoelectronic properties of the final polymer involving intramolecular charge transfer interactions[11,12]. In addition, the CN group is known to be a strong electron acceptor, and charge-transfer interactions are widely observed between metal ions and cyano groups[13,14]. On this point, we tried to incorporate luminescent metal ions (europium Eu^{+3} and ytterbium Yb^{+3}) into the polymer matrix in order to observe the effect of complexation on the optical properties of the complexes. The chemical structures of the new monomers and polymers were confirmed by IR and NMR techniques, and their relative molar masses were measured by LC-MS and SEC respectively. In addition, their thermal stability, electrochemical behaviour, liquid crystallinity and electronic properties were all studied and will be reported in this paper.

2. EXPERIMENTAL

2.1 Chemicals & Reagents
The chemicals, reagents and solvents used in this study were supplied by Sigma Aldrich, Fisher Scientific and Fluka. All the materials, anhydrous solvents, and reagents were used without further purification, unless specified.

2.2 Instrumentation
Attenuated total reflectance (ATR) infrared spectroscopy was performed on all samples using a diamond crystal Thermo Scientific Nicolet iS5 iD5 ATR instrument. Gas/liquid chromatography-mass spectrometry (GC-MS and LC-MS) were used to determine the molecular masses of the prepared monomers. GC-MS measurements were recorded using an Agilent Technologies 5973 network mass-selective detector and an Agilent technologies MSD Chemstation D.02.00.275. ^{1}H, ^{13}C NMR measurements were performed using a Bruker 400 MHz spectrometer. Molecular masses of the polymers were measured by size-exclusion (gel-permeation) chromatography (SEC), using THF as eluent (1mL/min) at room temperature and 380 nm detection wavelength, and standard polystyrene samples were used for calibration. The thermal stability of the polymers was investigated by thermogravimetric analysis (TGA) using a Mettler Toledo balance with a heating rate of 10 °C min^{-1} under N_2 atmosphere. Phase transition temperature measurements were carried out by differential scanning calorimetry (DSC) and hot-stage polarised optical microscopy (POM). The DSC equipment was a Mettler Toledo thermal analyser with Mettler TC 10A processor based on a TA 3000 system with Graphware TA 72 software. Measurements were done under N_2 with heating rates of 10 °C min^{-1} for polymers and 5 °C min^{-1} for monomers. Polarised hot-stage optical microscopy (POM) (Linkam HFS 91, Nikon microscope with a Linkam THMS-600 heating stage) was used to investigate the liquid crystal mesophases of the prepared monomers.
UV-Visible (UV-vis) spectra were recorded on a Cary 100 UV-Vis spectrophotometer. HOMO-LUMO energy levels and electrochemical band-gaps ($E_{g.ec}$) were determined by cyclic voltammetry under an N_2 atmosphere. Photoluminescence measurements were performed on a VARIAN fluorimeter at room temperature using different excitation wavelengths. Double-layer light-emitting diodes (PLEDs) with the configuration ITO/PEDOT:PSS/Polymer/Al were fabricated on indium-tin oxide (ITO)-coated glass slides (surface resistivity 70-100 Ω/sq) cleaned in ultrasonic baths of water, acetone and isopropanol. A hole injection layer (HIL) of poly(ethylenedioxythiophene polystyrenesulfonate) (PEDOT:PSS) was spin-coated on top of the ITO glass and dried at 80°C for one hour under vacuum. Polymer solutions (5 mg/mL) were spin-coated from THF solutions onto the HIL. The Al metal cathode was vacuum-deposited onto the emissive polymer layer at a pressure below 10^{-5} Torr. A shadow contact mask having a 2 mm inside hole diameter was used to pattern metal contacts for the diode fabrication.
I-V measurements were carried out on the diode devices using a Keithley 230 programmable voltage source and a Keithley 485 picoammeter. Data acquisition for I-V measurements was achieved by connecting both instruments to a computer with data acquisition software. Electrical contacts were made to the Al (cathode) and ITO (anode). Applied voltages were between -5 and +12 V. Electroluminescence measurements were recorded with the cell fixed inside the fluorimeter, ensuring the diode was as close as possible to the detector slit. Measurements were made at room temperature in ambient atmosphere, with an applied potential of about 8-12 V for each reading.

2.3 Organic Synthesis
2.3.1 Synthesis of Precursor Molecules

4,4-diformyl diphenoxydodecane precursor 1 was prepared as follows: In a typical synthesis, 4-hydroxybenzaldehyde (3.05 g, 0.025 mol) was dissolved in 50 mL anhydrous dimethylformamide (DMF) at 80°C under N_2 atmosphere. To this solution, anhydrous potassium carbonate (K_2CO_3) (5.17 g, 0.375 mol) was added, followed by dropwise addition of 1,12-dibromododecane (4.05 g, 12.25 mmol) and the reaction mixture was stirred at 150°C for 5 h. After cooling to room temperature, the mixture was poured into 500 mL of distilled water. The precipitate was collected by filtration and washed with 5% aqueous $NaHCO_3$ and then distilled water. The crude product was recrystallised from ethanol. Yield was 4.0 g (80%); m.p.: (78-79)°C; ^{1}H NMR (400 MHz, $CDCl_3$, ppm): 9.88(s, -CHO), 7.82 (4H, d, aromatic proton, J = 8.7 Hz), 6.99 (4H, d, aromatic proton, J = 8.7 Hz), 4.04 (4H, t, Ar-O-αCH_2-, J = 6.6 Hz), 1.835-1.785 (4H, quint, β CH_2-), 1.49-1.44 (4H, quint, CH_2-, J = 7.5 Hz), 1.37-1.3(12H, m, CH_2-). ^{13}C NMR (400MHz, $CDCl_3$, ppm): 190.82, 164.26, 131.99, 129.75, 114.74, 68.42, 29.56, 25.98; GC-MS: exact mass 410 eluted at 22.11 min using hexane:ethyl acetate 3:1 v/v as eluent; ATR ν, cm^{-1}: 2920, 2850, 2740, 1685, 1593, 1507, 1261, 832.
4,4-diformyl diphenoxyoctane precursor 2 was prepared by reacting 1,8-dibromooctane with 4-hydroxy-benzaldehyde, following the same procedure as for precursor 1. Yield: 85%; m.p.: 82-84°C; ^{1}H NMR (400 MHz, $CDCl_3$, ppm): 9.80 (s, -CHO), 7.75, (4H, d, aromatic proton, J = 8.8 Hz), 6.91 (4H, d, aromatic proton, J = 8.8 Hz), 3.97 (4H, t, ArO-αCH_2-, J = 6.5 Hz), 1.79-1.72 (4H, quint, Ar-O-βCH_2-), 1.44-1.33 (8H, m, -CH_2-); ^{13}C NMR (400 MHz, $CDCl_3$, ppm): 190.84, 164.23, 132.01, 129.79, 114.75, 68.35, 29.25, 25.94;

GC-MS: exact mass 354 eluted at 23.514 min using hexane: ethyl acetate 3:1 v/v as eluent; ATR ν, cm^{-1}: 2939, 2851, 2756, 1686, 1594, 1509, 1263, 831.

Synthesis of 1,4-bis(4-formyl styryl)-2,5-bis(octyloxy)benzene

Precursor 3 was prepared by a procedure described elsewhere[15,16]. Yield: 2.8 g, (59.8%); m.p.: 122°C; ^{1}H NMR (400 MHz, $CDCl_3$, ppm) 10.03 (2H, s, CHO), 7.91 (4H, d, aromatic proton, J = 8.3 Hz), 7.71 (4H, m, aromatic proton), 7.64 (2H, d, =CH-), 7.22 (2H, d, -HC=) 7.17 (2H, s, aromatic proton), 4.11 (4H, t, ArO-αCH_2, J = 6.4 Hz), 1.93 (4H, quint, ArO-βCH_2), 1.59 (4H, quint, -CH_2-), 1,48-1.34 (16H, m), 0.91 (6H, t, CH_3 terminal); ^{13}C NMR (400 MHz, $CDCl_3$, ppm): 191.96, 151.78, 144.37, 135.58, 130.63, 128.26, 127.28, 111.12, 69.86, 32.32, 30.10, 29.84, 29.76, 26.68, 23.09, 14.52; LC-MS: exact mass (m/z 594.5). ATR cm^{-1}: 2920, 2851, 2730, 1691, 1592, 1563, 1204, 858.

2.3.2 Synthesis of Thiophene Liquid Crystalline Monomers ($THLC_{12}$, $THLC_8$, THLC3 and THLC4)

Since the synthetic procedures for preparation of the thiophene Schiff-base monomers were the same, a typical procedure for the preparation of monomer one $THLC_{12}$ is taken as an example (Scheme 1). Into a three-necked round bottom flask equipped with a condenser, argon inlet-outlet tube, Dean-Stark apparatus and magnetic stirrer, 1 equiv. of **4,4-diformyl diphenoxydodecane precursor** 1 (0.41 g, 1 mmol), and 2 equiv. of 2-aminothiophene-3-carbonitrile (ATHCN) (0.248 g, 2mmol) were charged. After purging the reaction vessel with argon gas, a mixture of 1:1 v/v of isopropyl alcohol:chloroform and catalytic amount of trifluoroacetic acid TFA was added by glass syringe to the reaction vessel. The reaction mixture was then stirred for 48 h at 80-90°C, and the by-product water was removed during the reaction *via* the Dean-Stark apparatus. The solid product was filtered off and washed repeatedly with isopropanol (IPA), recrystallised from toluene, and dried in vacuum for 24 h. **$THLC_{12}$** (0.45 g) was obtained as yellow powder with 72% yield.

m.p, 166-168°C; LC-MS: exact mass (m/z 622.4); ^{1}H NMR (400 MHz, $CDCl_3$, ppm): 8.47 (s, 2H, azomethine protons), 7.94 (d, 4H, aromatic protons, J = 8.8 Hz), 7.14 (d, 2H, thiophene ring, J = 5.8 Hz), 7.06 (d, 2H, thiophene ring, J = 5.8 Hz), 7.0 (d, 4H, aromatic protons, J = 8.8 Hz), 4.06 (t, 4H, ArO-αCH_2, j = 6.5 Hz), 1.84 (quint, 4H, ArO-βCH_2), 1.49 (quint, 4H, aliphatic protons), 1.38 (m, 12H aliphatic protons); ^{13}C NMR (400 MHz, $CDCl_3$, ppm): 164.20, 163.20, 131.77, 127.66, 120.13, 114.97, 104.75, 68.37, 29.55, 29.13, 26.01; ATR ν, cm^{-1}: 3105, 2922, 2852, 2224, 1593, 1562, 1521, 1252, 837, 730-648.

$THLC_8$ was prepared by the reaction of one equiv. (0.354 g, 1 mmol) of 4,4-diformyl diphenoxyoctane precursor 2 and two equivs. (0.248 g, 2 mmol) of 2-aminothiophene-3-carbonitrile, following the same procedure as for $THLC_{12}$.

Yield: 70%; m.p: 180-182; LC-MS: exact mass (m/z 566); ^{1}H NMR (400 MHz, $CDCl_3$, ppm): 8.47 (s, 2H, azomethine protons), 7.94 (d, 4H, aromatic protons, J = 8.8 Hz), 7.14 (d, 2H, thiophene protons, J = 5.8 Hz), 7.06 (d, 4H thiophene protons, J = 5.5 Hz), 7.0 (d, 4H, aromatic protons, J = 9.0 Hz), 4.07 (t, 4H, ArO-αCH_2, J = 6.5 Hz), 1.86 (quint, 4H, ArO-βCH_2), 1.52-1.43 (m, 8H, aliphatic protons); ^{13}C NMR (400 MHz, $CDCl_3$, ppm): 164.19, 163.16, 160.55, 131.77, 127.50, 120.32, 114.97, 104.77, 68.29, 29.26, 25.94; ATR ν, cm^{-1}: 3106, 2940, 2855, 2225, 1593, 1561, 1522, 1255, 838, 730-649.

THLC3 was prepared by the reaction of one equiv. (0.4 g, 0.673mmol) of 1,4-bis(4-formylstyryl)-2,5-bis(octyloxy)benzene precursor 3 and two equivs. (0.168 g, 1.3468mmol) of 2-amino thiophene-3-carbonitrile, following the same procedure as for $THLC_{12}$.

Yield: 83%; m.p: 187-188°C; LC-MS: exact mass (m/z 806); ^{1}H NMR (400 MHz, $CDCl_3$, ppm): 8.53 (s, 2H, azomethine protons), 7.99 (d, 4H, aromatic ring, J = 8.5 Hz), 7.67 (s, 2H, aromatic protons), 7.64 (d, 4H, aromatic protons, J = 9.0 Hz), 7.25 (d, 2H, =CH-), 7.21 (d, 2H, -HC=), 7.18 (d, 2H, thiophene protons, J = 5.5 Hz), 7.12 (d, 2H, thiophene protons, J = 5.8 Hz), 4.12 (t, 4H, ArO-αCH_2, J = 6.5 Hz), 1.94 (quint, 4H, Ar-O-βCH_2), 1.61 (quint, 4H, aliphatic protons), 1.4-1.35 (m, 16H, aliphatic protons), 0.92 (t, 6H, terminal CH_3); ^{13}C NMR (400 MHz, $CDCl_3$, ppm): 163.6, 160.4, 151.4, 142.5, 133.7, 130.2, 127.0, 121.1, 114.8, 110.7, 105.7, 69.5, 31.9, 29.4, 26.3, 22.7, 14.2; ATR ν, cm^{-1}: 3081, 2914, 2853, 2231, 1588, 1552, 1507, 1200, 851, 746-649.

THLC4 was prepared by the reaction of one equiv. (0.301 g, 1 mmol) of **4,4-diformyltriphenylamine** and two equiv. (0.248 g, 2 mmol) of 2-amino thiophene-3-carbonitrile, following the same procedure as for $THLC_{12}$. Yield: 87.7%, 0.45 g; m.p: decomposes; LC-MS: exact mass (m/z 513); ^{1}H NMR (400 MHz, $CDCl_3$, ppm): 8.48 (s, 2H, azomethine protons), 7.89 (d, 4H, aromatic ring, J = 8.5 Hz) 7.41 (d, 2H, aromatic protons, J = 8.0 Hz), 7.2 (d, 4H, aromatic protons, J = 8.8 Hz), 7.16 (m, 3H, aromatic protons), 7.08 (d, 2H, thiophene ring, J = 5.5 Hz), 7.05 (d, 2H thiophene ring, J = 5.8 Hz); ^{13}C NMR (400 MHz, $CDCl_3$, ppm): 163.9, 162.4, 145.8, 140.8, 131.2, 130.1, 129.4, 127.8, 126.8, 126.0, 122.7, 100.0, 86.0; ATR ν, cm^{-1}: (3061, 2920, 2220, 1581, 1522, 1501, 1283, 825, 721-641).

2.3.3 Polymerisation of thiophene monomers $THLC_{12}$, $THLC_8$, THLC3 and THLC4

The polymers were prepared by chemical oxidation of the monomers using anhydrous $FeCl_3$ (Sigma-Aldrich, 99.99%), based on Sugimoto's procedure[17]. Since the reaction procedures for the polymerisation of these monomers were the same, a typical procedure for the preparation of polymer **PTAZ1** is taken as an example (Scheme 1). Anhydrous $FeCl_3$ (0.33 g, 1.54 mmol) was suspended in 20 mL of dry $CHCl_3$ under a pure nitrogen atmosphere, and a solution of $THLC_{12}$ (0.32 g, 0.514 mmol) in dry $CHCl_3$ (20 mL) was added dropwise under vigorous stirring. The mixture was stirred for 24 h at room temperature under nitrogen. The dark solution was poured into distilled methanol (50 mL), and the black precipitate was filtered. The precipitate was then immersed in 10 mL of methanol containing 1%, v/v of hydrazine and stirred for 24 h at room temperature. Residual traces of Fe(III) salts, oligomers, unreacted monomers and low molar mass fractions of polymer were removed by Soxhlet extraction using a mixture of methanol:acetone (1:1) for 24 h. Polymer PTAZ1 was collected as a brown powder (0.2 g, 62%) after drying for 24h under vacuum. ^{1}H NMR (400 MHz, $CDCl_3$, ppm): 8.48 (s, azomethine protons), 7.95 (d, aromatic ring, J = 8.8 Hz), 7.55 (s, thiophene ring), 7.15 (d, thiophene protons, J = 5.8 Hz), 7.04 (d, aromatic protons, J = 9.0 Hz), 4.1 (t, ArO-αCH_2, J = 6.5 Hz), 1.79 (quint, ArO-βCH_2), 1.50-1.183 (m, aliphatic protons); ATR ν, cm^{-1}: 3100, 2939, 2866, 2205, 1600, 1570, 1507, 1261, 832, 730-626.

PTAZ2 was prepared by the chemical oxidation of $THLC_8$ (0.2 g, 0.35mmol) following the same procedure as for PTAZ1. Yield: 0.165 g, 82%; ^{1}H NMR (400 MHz, $CDCl_3$, ppm): 8.38 (s, azomethine protons), 7.84 (d, aromatic protons, J = 8.8) 7.45 (s, thiophene ring), 7.04-6.90 (aromatic & thiophene protons), 3.68 (t, ArO-αCH_2), 1.79(quint, ArO-βCH_2), 1.18(m, aliphatic protons); ATR ν, cm^{-1}: 3050, 2930, 2856, 2218, 1590, 1562, 1508, 1249, 832, 722-624.

PTAZ3 was prepared by chemical oxidation of THLC3 (0.3 g, 0.372 mmol) following the same procedure as for PTAZ1. Yield: 0.2 g, 66.6%; ^{1}H NMR (400 MHz, $CDCl_3$, ppm): 8.25 (s, azomethine protons), 8.0 (d, aromatic protons) 7.49 (s, 2H thiophene ring), 7.12-

7.10 (m, aromatic protons), 4.01 (t, ArO-αCH$_2$), 1.9 (quint, ArO-βCH$_2$), 1.56-1.25 (m, aliphatic protons), 0.9 (t, terminal CH$_3$); ATR ν, cm^{-1}: 3010, 2925, 2854, 2205, 1598, 1554, 1508, 1194, 832, 720-614.
PTAZ4 was prepared by chemical oxidation of THLC4 (0.3 g, 0.584 mmol) following the procedure for PTAZ1. Yield: 0.15 g, 50%; ^{1}H NMR (400 MHz, CDCl$_3$, ppm): 8.40 (s, azomethine protons), 7.92 (d, aromatic ring) 7.51(s, thiophene ring proton), 7.4-735 (m, aromatic protons), 7.21-6.83 (m, aromatic protons); ATR ν, cm^{-1}: (3061, 2920, 2220, 1600, 1522, 1501, 1283, 825, 721-641).

3. RESULTS AND DISCUSSION

3.1 Organic Synthesis and Structural Characterisation

Thiophene Schiff-base monomers (THLC$_{12}$, THLC$_8$, THLC3 and THLC4) were prepared as described above, analogously to a published procedure[18] (**Scheme 1**). The deactivating effect of the cyano group of the ATHCN monomer leads to a significant decrease in the activity of the amine group, and this is why the coupling reactions affording symmetrical bis-azomethine proceeds slowly and with relatively small yield. However, thiophene azomethine monomers were obtained in sufficient yield by running the condensation reaction in a mixed solvent system. The thiophene azomethine monomers were obtained as pale to dark yellow solids for **THLC$_{12}$** and **THLC$_8$**, and as light to dark orange solids for **THLC3 and THLC4**, respectively. They were all soluble in the common polar solvents THF, DMF, DMSO, and also in CHCl$_3$. ATR spectra for all the monomers presented peaks between 1581-1593 cm^{-1} due to the CH=N linkages formed by the condensation reaction. The sharp single peak located at 2220-2231 cm^{-1} belongs to the CN groups. Peaks in the 2855-3080 cm^{-1} range correspond to the aliphatic and aromatic C-H stretching vibrations. The strong absorption peaks from 1490-1562 cm^{-1} correspond to C=C aromatic vibrations, while the peaks at 1288, 1200-1255 cm^{-1} are attributed to the C-N of TPA and C-O-C linkages, respectively. All the monomers showed characteristic bands below 730 cm^{-1} due to the C-S bond vibrations in the thiophene rings.

^{1}H, ^{13}C, HSQC and DEPT NMR spectra of the thiophene azomethine monomers showed the following main features: the imine protons exhibited a singlet at 8.53-8.47 ppm, whereas the doublet located at 8.0-7.75 ppm and the one at 7.14-7.06 ppm were attributed to the protons of the aromatic and thiophene rings, respectively. The protons ortho to the azomethine linkages produced a doublet at 7.99 ppm in the case of THLC3 and at 7.89 ppm in the case of THLC4. Peaks between 2.25-2.21 ppm in the spectra of THLC3 were attributed to the aliphatic -C=C- in the aromatic backbone of the monomer. Triplet peaks around 4.05 ppm belonged to ArO-αCH$_2$ for (THLC$_{12}$, THLC$_8$, and THLC3), and while the peaks located at 1.9-1.23 ppm were due to the aliphatic protons. The number of protons corresponding to each resonance signal based on integration of the peaks in the ^{1}H-NMR spectra were in good agreement with the proposed structures for all the monomers.

Thiophene azomethine polymers were synthesised by oxidative polymerisation using anhydrous FeCl$_3$. Since the thiophene azomethine monomers used in this study were symmetrical, there was no need to check whether the polymerisation proceeded by a head-head or head-tail mechanism, and in our case position five was the most favourable one for the polymerisation. The colours were dark red-brown for PTAZ1 and PTAZ2, dark yellow for PTAZ3 and shiny black for PTAZ4.
Structures of the polymers were confirmed by ATR spectroscopy, ^{1}H-NMR and HSQC techniques. Most polymers showed a new characteristic singlet peak located at 7.55-7.4 ppm, corresponding to the proton at carbon number 4 of the thiophene ring in the polymer backbone. This new peak provided confirmation that the polymerisation took place at position five of the thiophene ring. Azomethine protons were observed between 8.45-8.35 ppm in the spectrum, peaks belonging to the aromatic protons located at 7.9-6.90 ppm, while peaks at 4.1-3.68 ppm were due to ArO-αCH$_2$ for PTAZ1-PTZA3. Signals for the aliphatic protons were observed between 1.9-1.23 ppm, while terminal methyl groups were as usual around 0.9-0.8 ppm.

3.2 Solubility Tests and GPC studies

Thiophene azomethine polymers (PTAZ1-PTAZ4) were partly soluble in polar solvents such as THF, DMF and DMSO. The molar masses for all the prepared polymers and random copolymers were studied by SEC (GPC) using polystyrene standards. The results showed relatively high molar masses (M_w = 14000-18000; M_n = 12670-16500) for the soluble fractions. The data are summarised in **Table 1.**

Table 1. M_n, M_w and PDI data for the prepared polymers, obtained by GPC at room temperature.

Code	Mn	Mw	PDI
PTAZ1	13500	15000	1.11
PTAZ2	12650	14000	1.10
PTAZ3	16500	18000	1.09
PTAZ4	14500	17250	1.18

3.3 Thermal Stability Studies

The thermal stabilities of the prepared polymers were evaluated by TGA, considering the onset of thermal decomposition (T_o) and the endset of thermal decomposition (T_{max}) the temperature corresponding to the maximum rate of weight loss. All the polymers were examined under nitrogen up to 600°C; the data are shown in **Table 2**.

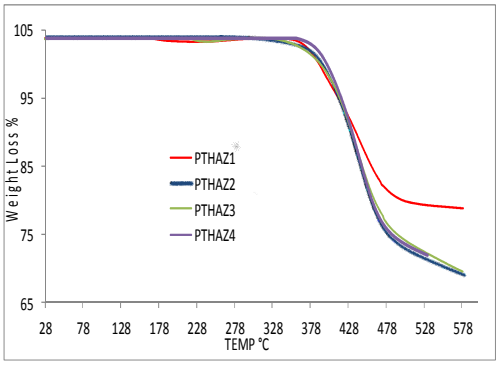

Figure 1. TGA curves for polymers PTAZ1-PTAZ4, under N_2.

The TGA data of polymers PTAZ1-PTAZ4 (**Figure 1**) show very good thermal stability. At 410°C, PTAZ4 underwent only 2.5% weight loss. PTAZ1, with twelve methylene spacers, showed less thermal stability than the other polymers (T_o = 375°C, 3.5% loss), which was expected because the methylene groups tend to increase the thermal degradation at temperatures higher than 350°C.
PTAZ2, with eight methylene spacers, commenced weight loss at 390°C, whereas the fully-conjugated PTAZ3 with aliphatic side chains showed a T_o of 385°C. The maximum rates of weight loss at temperatures higher than 400°C were almost irrespective of the polymers' chemical structures. For example, PTAZ1 showed about 20% weight loss at T_{max}=476°C, while for PTAZ2 with eight methylene spacers, the weight loss was about 25% at T_{max}=472°C. PTAZ3 with an aliphatic side chain suffered 20% weight loss at T_{max}=482°C, whereas PTAZ4 with triphenylamine moieties had around 23% weight loss at 490°C.

Table 2. TGA data from the TGA thermograms of polymers PTAZ1-4.

Code	T_o °C	T_{max} °C	% char at T_{max}
PTAZ1	357	476	80
PTAZ2	390	472	75
PTAZ3	385	482	80
PTAZ4	410	490	77

3.4 Liquid Crystalline Properties

The LC properties of the products were analysed by calorimetry and polarised optical microscopy, as will be discussed below.

3.4.1 Differential Scanning Calorimetry (DSC)

DSC traces for $THLC_{12}$ exhibited two endothermic peaks during the heating scan; the first one between 135-148°C was attributed to the phase change from solid crystal to nematic LC phase (see **Figure 2**). The second phase change during the heating scan was located at 160°C and was assigned as a melting process. The cooling scan for $THLC_{12}$ showed only one exothermic peak starting from 148 to 122°C with a maximum at 145°C, correlated to the emergence of a new LC phase. Thiophene azomethine monomer $THLC_8$ presented a phase change at 180°C due to its melting process, and a corresponding exothermic peak was observed at 164°C in the cooling scan. THLC3, with an octyloxy side-chain, exhibited an endothermic peak at 138°C that probably belonged to one of the LC phases, and a melting peak at 188°C. The cooling scan of THLC3 revealed a broad exothermic peak (134-117°C) due to the phase change from isotropic to crystalline phase. Thiophene-triphenylamine azomethine monomer THLC4 showed no evidence of LC organisation, either in the DSC or POM, due to the tetrahedral configuration of the aromatic rings in TPA. The only DSC feature was at about 90°C, which has not yet been assigned.

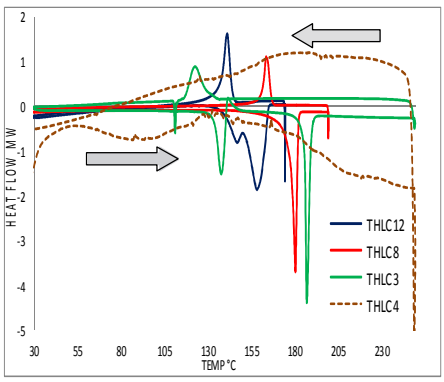

Figure 2. DSC curves for the thiophene azomethine monomers.

DSC traces for the prepared thiophene azomethine polymers are shown in **Figure 3**, and the T_g values in **Table 3**. PTAZ1 (T_g~100°C) and PTAZ2 (T_g~125°C) showed exothermic peaks at 358°C and 395°C corresponding to the onset of decomposition. Small endothermic peaks were observed for PTAZ1 at 110, 130 and 235°C respectively, and were tentatively attributed to the interconversion of mesomorphic forms. No equivalent peaks were clearly identifiable for PTAZ2. PTAZ3 (T_g~120°C) showed a small endothermic peak at around 135°C, assigned as a LC phase. PTAZ4 (T_g~185°C) shows no features characteristic of LC phases, while the exothermic peak located at 565°C probably relates to the oxidation of the aromatic backbone of this stable polymer.

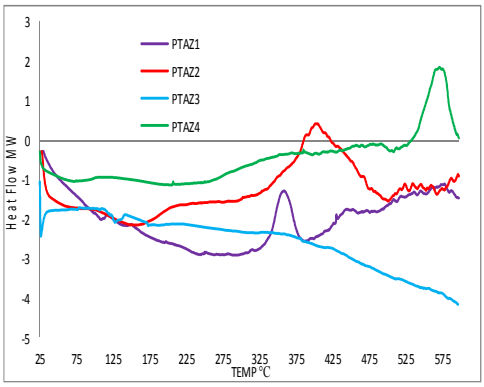

Figure 3. DSC traces for the prepared thiophene azomethine polymers.

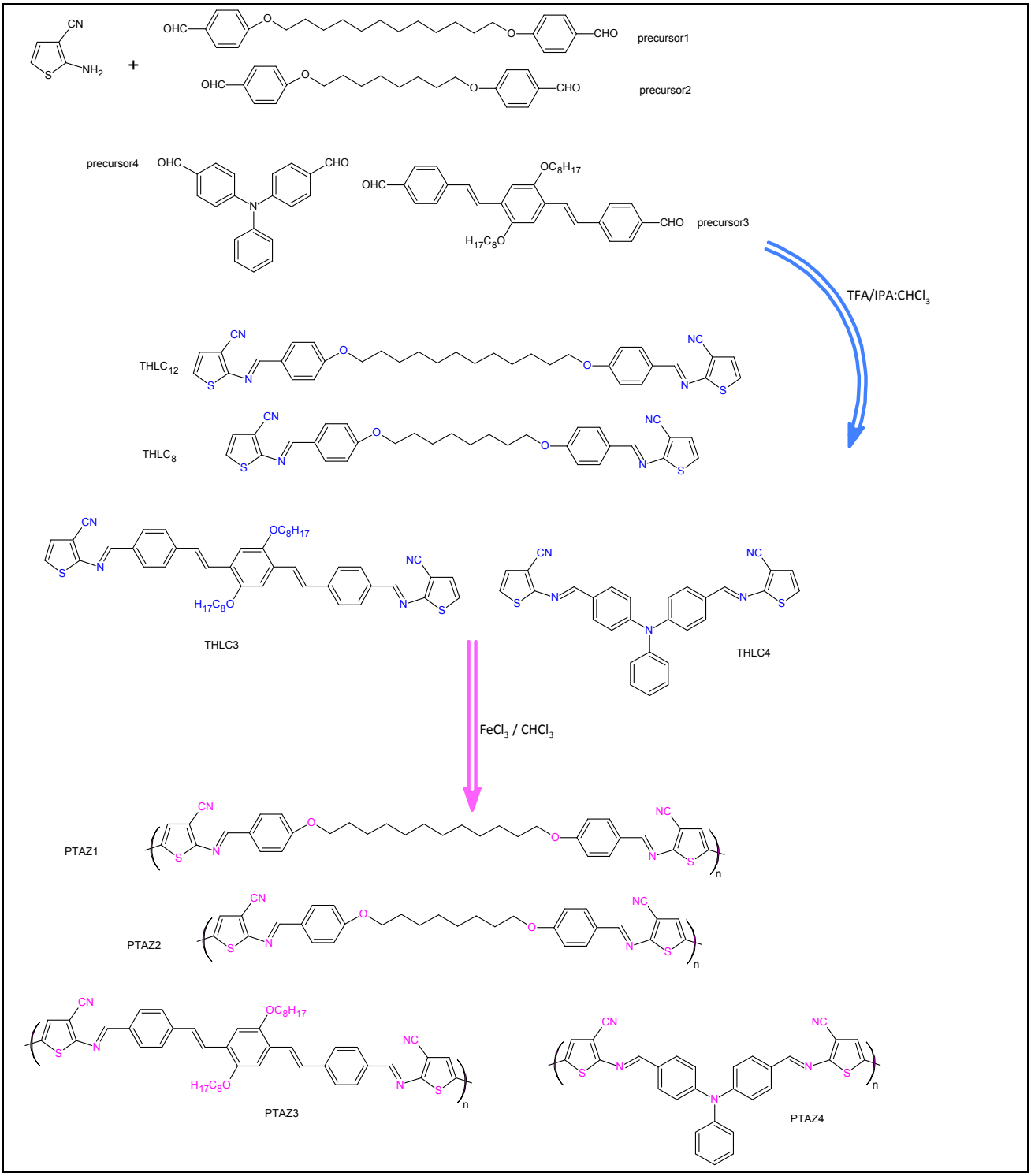

Scheme 1. Chemical synthesis of the thiophene azomethine monomers and polymers

3.4.2 Hot Stage Polarised Microscopy Studies

Polarised optical microscopy (POM) was performed to confirm the transition temperatures obtained by DSC studies and to indicate the type of mesophases present in the studied materials. Only the monomers were examined in this study, not the polymers, due to their strong colour and structural rigidity (nitrile groups increased the rigidity of the polymers and made optical observation impossible). All the monomers were heated (5 °C min^{-1}) on glass slides to melting on the hot stage microscope, and the phase changes were examined during the cooling scan (3 °C min^{-1}). POM photographs (**Figure 4**) for the prepared thiophene azomethine monomers showed a focal-conic texture (nematic phase) for $THLC_{12}$ at temperatures between 160°C and room temperature. $THLC_8$ revealed a phase change after cooling to 172°C, representative of smectic LC phases with short-range positional order. Long-range positional order was observed by POM in the same range of temperatures as in the DSC during cooling scan of THLC3 film on glass slide. The texture of the monomer film is likely to be a (SmC) LC mesophase with oblique long-range positional order.

Table 3. Phase transition temperatures and visual observations of thiophene azomethine monomers and polymers from DSC and POM.

Code	Phase transition temperatures °C	POM observation	T_g °C
$THLC_{12}$	H: 135-148 FOT, 160 cr→n. C: 145 FOT	H: shows phase changes from cr→n→iso C: shows focal-conic texture of nematic LC phase	
$THLC_8$	H: 180 FOT cr→iso. C: 164	Phase change below 177 °C belonging to nematic LC phase	
THLC3	H: 138 FOT, 188 cr→iso. C:134-117 iso→sm C	H: shows phase change from cr→sm C: phase change iso→sm.C, oblique long positional order	
THLC4	H: 90 FOT	No LC phase was observed	
PTAZ1	H: ~100, 110, 130, 235	No observation was made on these polymers due to sample limitations	100
PTAZ2	H: 125-180 broad endotherm		125
PTAZ3	H: 120, 135		120
PTAZ4	H: 185		185
H: heating, C: cooling, cr: crystalline, iso: isotropic, n: nematic, sm: smectic, FOT: first order transition			

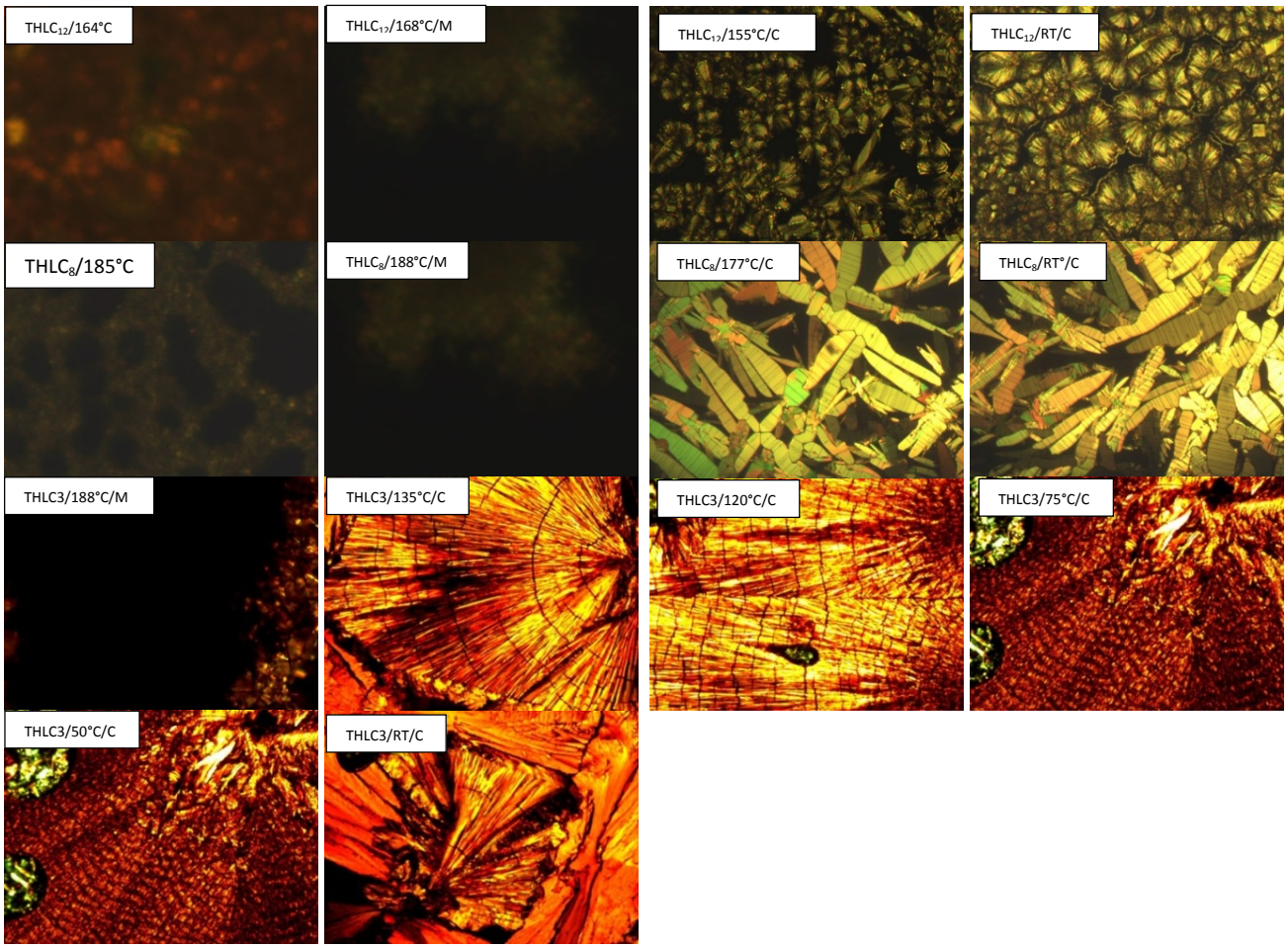

Figure 4. POM photographs for the thiophene azomethine monomers after cooling from their melting points to room temperature.

3.5 Electrochemical Analysis

To investigate the electrochemical behaviour and to estimate the HOMO and LUMO energy levels as well as the electrochemical energy gaps of the prepared polymers, **c**yclic **v**oltammetry was employed. Measurements were recorded in a conventional three electrode cell system using a Uniscan (UiChem Version 3.44.31.45, PG 581) instrument. A platinum rod was used as counter electrode and a small platinum disk as working electrode while a sealed Ag/Ag^+ electrode was used as a reference. Cyclic voltammograms were obtained by dissolving 2 mg of the prepared polymers in THF solution following by drop-casting onto the surface of the working electrode. 0.1 M tetrabutylammonium hexafluorophosphate in 50 mL CH_2Cl_2 was the supporting electrolyte. Ferrocene (Fc) was used to calibrate the potential of the reference electrode. The HOMO-LUMO energy values of the prepared polymers were calculated, based on a value of -4.8eV for ferrocene/ferricenium ion (Fc/Fc^+) with respect to the zero vacuum level. The following equations were used to evaluate the HOMO and LUMO energy levels as well as the electrochemical band gap ($E_{g.ec}$).

$$HOMO\ (eV) = -e\{(E_{onset}) + 4.54\}$$

$$LUMO\ (eV) = -e\{(E_{onset})_{red} + 4.54\}$$

$$E_{g.ec} = (E_{onset})_{ox} - (E_{onset})_{red}$$

where $(E_{onset})_{ox}$, $(E_{onset})_{red}$ are the measured oxidation and reduction potentials relative to an Ag/Ag^+ electrode.

Table 4 summarises the HOMO and LUMO energy levels and also the values of $E_{g.ec}$. Due to the presence of a free electron pair at the imine nitrogen atom belonging to the Schiff base linkages, all the polymers in this study underwent reversible oxidation processes between -1.6 and +2 V. The oxidative process was initiated by removing an electron, generating a radical cation which then reacted, either with other radical cations or with neutral molecules at the electrode-solution interface. The onset of PTAZ1 oxidation was +1.24V and reduction was -1.195V vs. Ag/Ag^+ which indicates a HOMO level of -5.78eV and a LUMO level of -3.34eV. PTAZ2 indicated almost the same data for onset of oxidation at +1.22 and -1.14V for the onset of reduction, corresponding to a HOMO level of -5.76eV and a LUMO level of -3.40eV. The fully-conjugated polymer (PTAZ 3) showed the onset of oxidation at +1.0V and reduction at -0.95 vs. Ag/Ag^+, implying a HOMO level of -5.54eV and a LUMO level of -3.59eV. PTAZ4 with triphenylamine moieties exhibited an onset of oxidation at +1.06V and onset of reduction at -1.08V, corresponding to a HOMO level of -5.6eV and a LUMO level of -3.46eV.

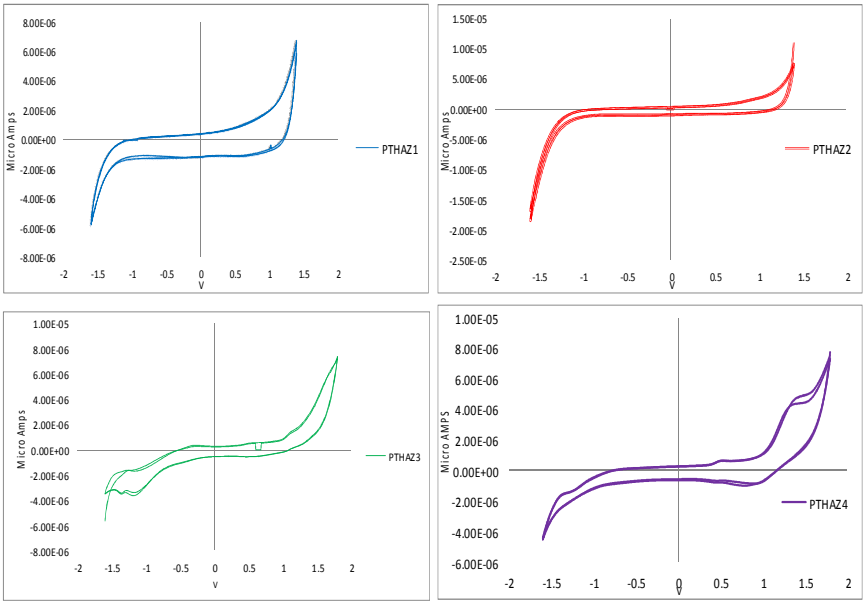

Figure 5. Cyclic voltammograms of the thiophene azomethine polymers in 0.1 M Bu_4NPF_6 in CH_2Cl_2.

Table 4. Electrochemical data for the thiophene azomethine polymers.

Polymer	E_{oxd} V	E_{red} V	$(E_{onset})_{ox}$ V	$(E_{onset})_{red}$ V	E_{HOMO} eV	E_{LUMO} eV	$E_{g.ec}$ eV
PTAZ1	+1.37	-1.6	+1.24	-1.19	-5.78	-3.34	2.43
PTAZ2	+1.36	-1.59	+1.22	-1.14	-5.76	-3.40	2.36
PTAZ3	+1.23	-1.09	+1.0	-0.95	-5.54	-3.59	1.95
PTAZ4	+1.29	-1.2	+1.06	-1.08	-5.6	-3.46	2.14

3.6 UV-Visible Absorption Spectra

The normalised UV–vis absorption spectra of the prepared thiophene azomethine polymers (both in solution and as thin solid films) are shown in **Figure 6 a-c**, and the data are presented in **Table 5**. In solvents with different polarities such as DMF, DMSO, and THF, the spectra of PTAZ1 and PTAZ2 showed three absorption peaks in the wavelength region of 270-600 nm (**Figure 6 a**). There was

only a small solvent polarity dependence of the absorption wavelength positions in these polymers. In the case of PTAZ1, the small shoulder located in the 293-296 nm wavelength region is attributed to the π-π* electronic transition of the phenyl rings, while the absorption peaks located at 362-368 nm are assigned to the π-π* transition along the polymer backbone, between the phenyl rings and thiophene moieties linked by -CH=N- double bonds.

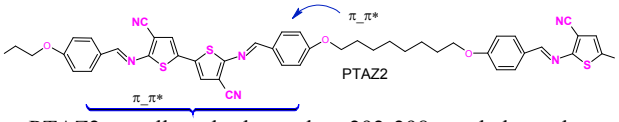

For PTAZ2, small peaks located at 292-298 nm belonged to π-π* transitions in the phenyl rings, while those related to the π-π* transitions along the polymer backbone were observed at 345-365 nm. Other peaks between 480-522 nm may be charge transfer (CT) bands due to internal charge transition between phenyl rings and CN acceptor groups. PTAZ3, a fully conjugated polymer with a push-pull system (see below) gave a small shoulder at 370 nm assigned to the high energy π-π* transition, while the broad peak located at 463-468 nm is attributed to the lowest energy π-π* transition (**Figure 6b**).

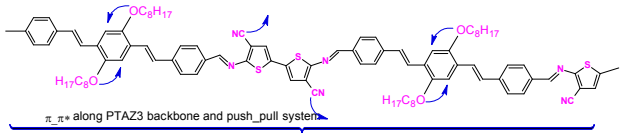

Polymer PTAZ4, which contains triphenylamine moieties along the polymer backbone, presented a small shoulder at around 369-373 nm attributed to a π-π* electronic transition in the triphenylamine units, while shoulders located at 436-438 nm corresponded to π-π* transitions along the polymeric backbone.

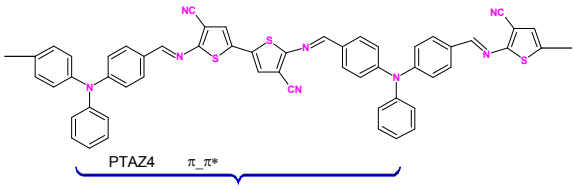

UV-visible spectra of the polymer thin films made by casting from THF solutions onto quartz plates are shown in **Figure 6d**. Polymers PTAZ1 and PTAZ2 showed bathochromic shifts (382, 377 nm) of about 15-20 nm compared to their solution counterparts. PTAZ3 showed a small shoulder at 388 nm which is shifted about 18 nm compared to the solution (370 nm), while the maximum located at 465 nm was shifted by about 17 nm to 482 nm in the solid film. The same behaviour was observed for PTAZ4 in solid film, the peak located at 438 nm in solution was found to be about 488 nm in a thin film cast on a quartz plate.

The optical band gaps were found to be in the range of 2.19 to 2.78 eV (calculated from the band edge positions using Planck's equation: $E_g = hc/\lambda_{edge}$) for the polymers in solution and in a narrower range, from 2.04 to 2.66 eV, for the polymer films. The largest band gap was found for PTAZ1, with a long flexible spacer. However, the E_g values of the polymeric films were lower than those of the corresponding polymers in solution, due to the more aggregated polymer chains in the solid state. The red shift of the absorption maxima from the longest wavelength characteristic of the chain segments containing azomethine linkages in the solid state with respect to solution can be explained by the fact that the intermolecular interaction in the solid polymer is stronger, and the chains better organised.

(a)

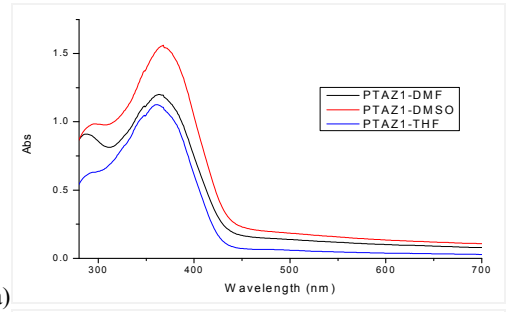

(b)

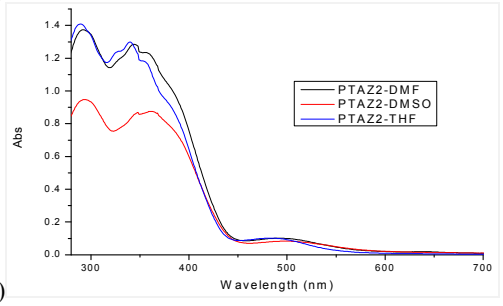

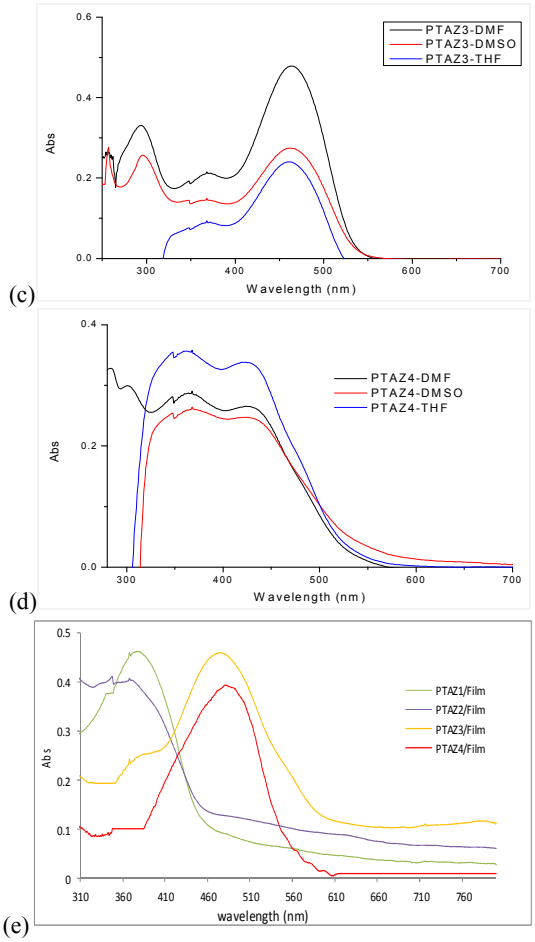

Figure 6. UV-visible absorption spectra of polymers PTAZ1-PTAZ4 in solution (6a-6d) and as solid films (6e).

Table 5. UV-visible absorption maxima for the thiophene azomethine polymers in the solid film and solution phases, and their calculated band gaps

Code	Soln. λ_{max} nm	Soln. λ_{edge} nm	Film λ_{max} nm	Film λ_{edge} nm	E_g Soln. eV	E_g Film eV
PTAZ1	296[s], 368	445	382	480	2.78	2.58
PTAZ2	298, 356	450	377	465	2.75	2.66
PTAZ3	370[s], 468	545	388[s], 482	600	2.27	2.06
PTAZ4	373[s], 438	565	488	605	2.19	2.04

The absorption edge, the onset of the lowest-energy band of the spectrum, moves to longer wavelengths for the polymer films relative to their solutions. Hence the conformation of the polymer chain may be very different, depending on the surroundings[19].

3.7 Fluorescence measurements

Fluorescence studies of the polymers under investigation were performed in three solvents with different polarities. Measurements were made at room temperature for both solid films and solutions: the data are collected in **Table 6** and the spectra are shown in **Figures 7a-d.** In solution, with excitation at suitable wavelengths, the polymers displayed strong fluorescence in the green-yellow-orange regions of the spectrum. Irradiation of PTAZ1 led to emission at 540, 538 and 532 nm in DMF, DMSO and THF solutions, respectively. More bathochromic shifting (594 nm DMF, 582 nm DMSO, and 537 nm THF) was observed for PTAZ2, analogous to PTAZ1 at the same excitation wavelength. This red shift can be explained by considering the lengths of the methylene spacers which were twelve in PTAZ1 and eight in PTAZ2. The different flexibilities of the two alkyl chains clearly affect the degree of π overlap between the C(2p) wavefunctions.

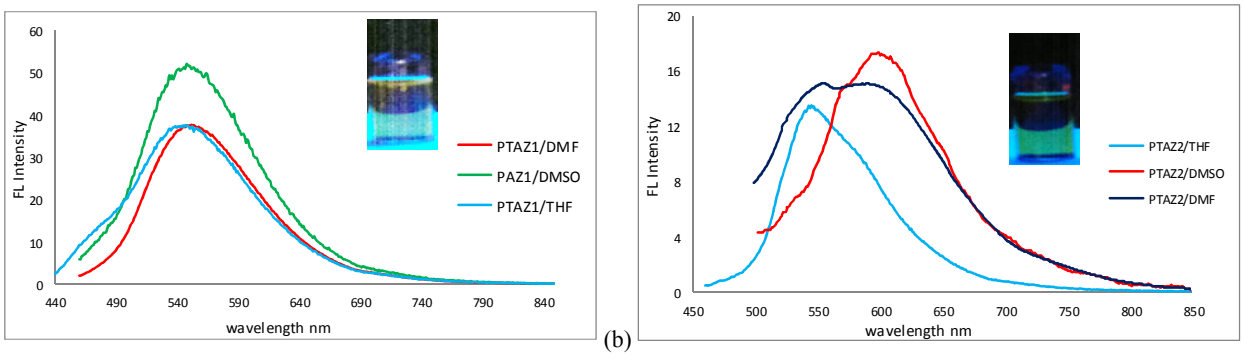

Figure 7. Fluorescence spectra of (a) PTAZ1 and (b) PTAZ2, solutions at 430 nm excitation wavelength.

Excitation of PTAZ3 at 480 nm gives almost the same emission wavelength (608 nm) in both DMF and DMSO, while the emission was blue-shifted (577 nm) by around 30 nm in the less-polar THF. Small shoulders at 716, 709 and 683 nm were also observed. Mirror-image symmetry was observed between the absorption and fluorescence spectra of a solution of PTAZ3 in DMF (**Figure 7c**). Mirroring only occurs when the geometries of the ground state S_o and the first excited state S_1 are similar, which is possible when there is rigidity in the polymer backbone. PTAZ4 showed emission peaks at 590, 600 and 557 nm in DMF, DMSO and THF respectively. This solvatochromic effect[20,21] generally occurs because the solvent is equilibrated with the ground state but not the excited state; this is often the case, and thus most absorptions are blue-shifted in polar solvents. Applying the same arguments to the emission of a long-lived excited state (where the solvent is equilibrated with the excited state and not with the instantaneously-produced ground state) indicates that most spectroscopic emissions in polar solvents will be red-shifted: the emission maxima of the polymers under study were indeed red-shifted as the polarity increased. The greatest solvatochromism was observed in PTAZ2 and PTAZ3. In a polar solvent such as DMF or DMSO, the emissive S_1 singlet state of the intramolecular charge transfer is strongly solvated, and its energy is therefore decreased. Consequently, the energy gap $E(S_1, S_2)$ is enlarged so that the coupling of the S_1 state directly to the ground state stays open, and intersystem crossing from the S_1 to the triplet (T) state is enhanced[22,23].

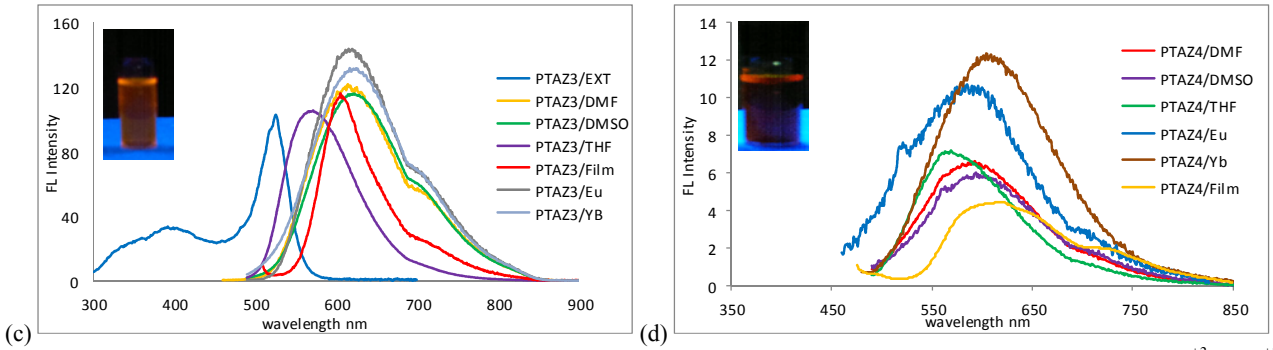

Figure 7. Fluorescence spectra for (c) PTAZ3 and (d) PTAZ4 (solution and film), before and after complexation with Yb^{+3} & Eu^{+3}.

The solid-state fluorescence spectra of PTAZ3 and PTAZ4 films under 450 nm excitation are shown in **Figure 7 c and d** (PTAZ1 and PTAZ2 were not examined). There was bathochromic shifting of the emission spectra with respect to those in solution.
An interesting observation was made after solution mixing of PTAZ3 and PTAZ4 with $EuCl_3$ and $YbCl_3$. The fluorescence from these polymers with 450 nm excitation was much more intense than that of the pure polymers before mixing with lanthanide ions (**Figure 7 c,d**). It was surmised that incorporating lanthanide ions might lead to increased organisation of the polymer chains *via* interaction (complexation) with the chromophoric groups along the polymer backbone and increase the similarity between the electronic states. It might also enhance the emission by increasing the rigidity of the polymer backbone and reducing wasteful intersystem crossing to the triplet state.

Table 6. Maximum fluorescent emission wavelengths for the polymers under study in solution and solid films.

Code	λ_{em} (nm) DMF	λ_{em} (nm) DMSO	λ_{em} (nm) THF	λ_{em} (nm) Film λ_{ex} = 450	λ_{em}(nm) with Eu^{+3}	λ_{em} (nm) with Yb^{+3}	Intensity
PTAZ1	540 λ_{ext} = 430	538	532	----------	-------	-------	-------
PTAZ2	594 λ_{ext} = 430	587	537	----------	-------	-------	-------
PTAZ3	608 λ_{ext} = 480	608	577	594	604 at 450	611 at 450	138, 129
PTAZ4	590 λ_{ext} =450	600	557	600	581 at 450	600 at 450	10, 12

3.9 Diode Device Characteristics and I-V Measurements

The polymer based PLEDs fabricated in this work had the structure (ITO / PEDOT:PSS / Polymer / Metal). The device was made by spin-coating a highly conductive and transparent organic layer of poly(3,4-ethylenedioxythiophene polystyrenesulfonate) onto transparent conductive indium tin oxide (ITO) glass (**Figure 8**).
Current-voltage graphs of the devices under investigation were measured by applying controlled voltages (-5 to +12 V) across the diodes and measuring the resulting current. The Schottky model was used to estimate the reverse-bias saturation current I_s and ideality factor n.

$I = I_s(\exp(V_d/nV_t) - 1)$

where n is the ideality factor (typically in the range 1 to 2), I is the diode current, V_d is the applied voltage and V_t is the thermal voltage (approximately 25.85 mV at 300 K), calculated as $V_t = kT/q$.

The forward bias current was obtained when the ITO glass electrode was positive and the aluminium electrode negative. The turn-on (or knee) voltage (the minimum one at which the device would conduct in forward-bias mode) was measured for all of the devices.

Table 7. Some important diode characteristics derived from the I-V graphs.

Code	V_o, V	ln (I) at V_o, A	ln(I_s) (intercept)	I_s, A	Ideality factor n
PTAZ1	7.34	-26.70	-29	2.543×10^{-13}	12.3
PTAZ2	7.00	-26.90	-29.5	1.542×10^{-13}	10.3
PTAZ3	6.20	-29.05	-30.25	7.287×10^{-14}	20.0
PTAZ4	8.00	-19.69	-23.00	1.026×10^{-13}	8.8

Table 7 shows the most important parameters derived from the I-V data for the devices (diodes 1-4). The ideality factor n is normally between 1 and 2 for conventional semiconductor devices, and it is clear that the apparent value of n is much greater here. This may indicate that the conventional models for charge injection and recombination are not applicable for the organic materials[24].

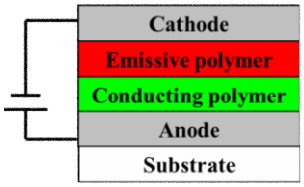

Figure 8. Diode device structure. (Conducting polymer: PEDOT:PSSA. Emissive polymer: PTHAZ1-4.)

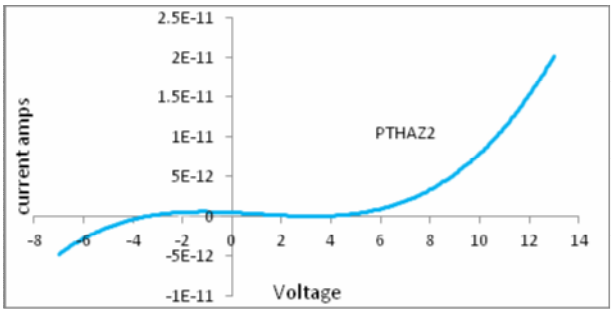

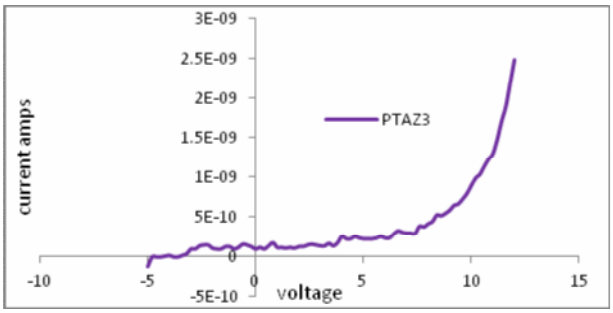

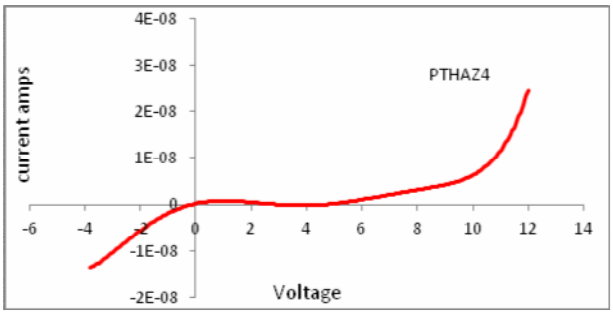

Figure 9. I-V curves for polymer diodes having (ITO/PEDOT:PSS/PAZ2/Al) diode structure.

Electroluminescence (EL) was measured for PTAZ3 and PTAZ4 only. The double layer devices produced electroluminescent spectra above the turn-on voltage (**Figure 10**) that were similar to their fluorescent spectra, indicating that the emission originated from the same singlet state S_1.

(a)

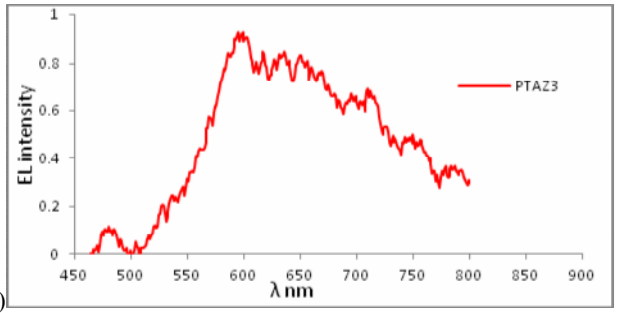

(b) 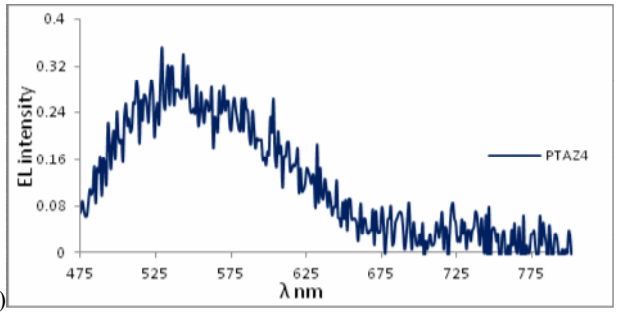

Figure 10. Electroluminescence spectra of (a) PTAZ3 and (b) PTAZ4 in an ITO/PEDOT:PSS/Polymer/Al diode structure.

4. MOLECULAR MODELLING STUDIES

Modelling computations were performed using **Scigress (FUJITSU)** software on a personal computer under Windows 7 XP Professional.

Theoretical absorption spectra of the polymers and their HOMO and LUMO energy levels were calculated by ZINDO using molecular geometries calculated by AMI geometry optimisation. ZINDO uses configuration interaction, so it can calculate the accurate excited-state wave functions necessary for electronic spectral calculations[25].

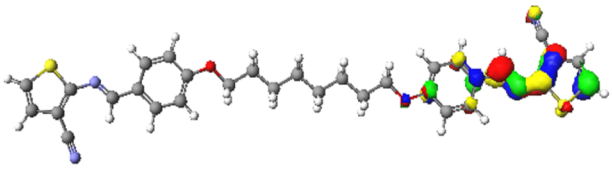

Figure 11. Geometry optimisation of PTAZ2 segments.

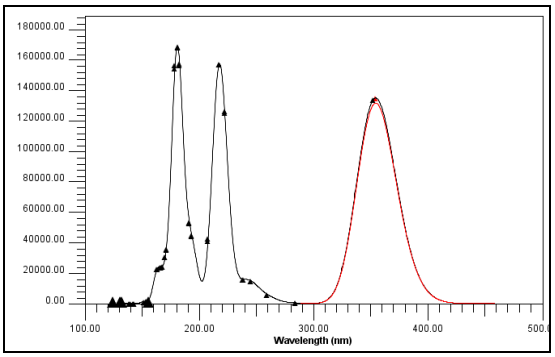

Figure 12. Calculated spectrum of PTAZ2 (chain segment).

The peak around 215nm in the calculated spectrum of PTAZ2 (**Figure 12**) relates to the cyano group, whereas the dominating low-energy transition essentially resides on the connecting azomethine bridge. The calculated spectrum agrees quite well with the observed one for PTAZ2 (**Figure 6a**).

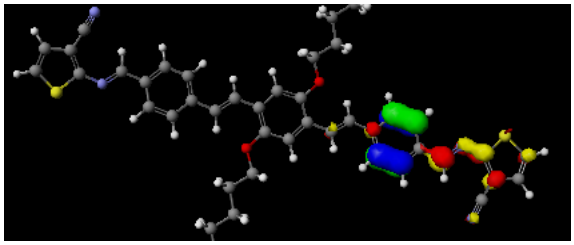

Figure 13. PTAZ3 optimised geometry using AM1.

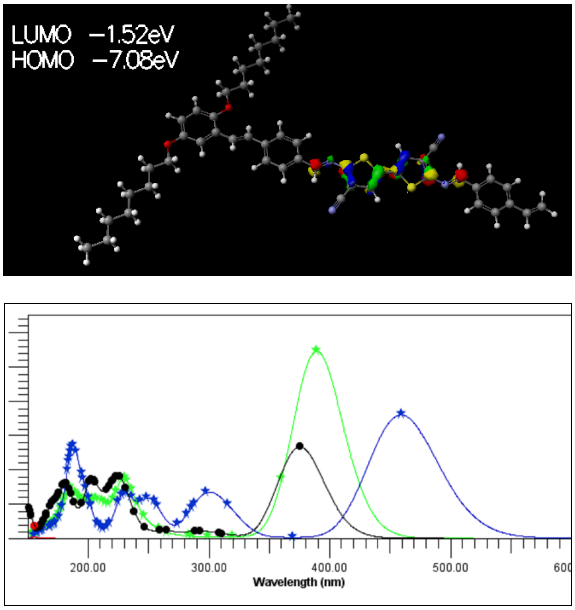

Figure 14. Calculated absorption spectra for two repeating units of PTAZ3.

In **Figure 14**, the starred curve peaking at 460 nm shows the predicted absorption of the dimer as a representative of a polymer chain, albeit one-dimensional and artificially capped with hydrogens. However, it serves as a good indicator of the way the spectrum develops with polymerisation: comparison with the solid film spectrum in **Figure 6** reveals good correspondence with the lowest transition around 450 nm. For the calculated spectrum, the weak higher transition appears at greater energy (300 nm) than the experimental one. **Figures 15 and 16** show that the dimer spectrum in which two molecules are simply coupled is significantly different to the monomer spectrum, and is more similar to the solution-based polymer spectra. In the latter, a small shoulder at low energy is evident (460 – 500 nm). It is not yet clear whether this is a remnant of the monomer or is due to a different conformation. (Rotation around the central bond linking the two thiophene rings would produce a more monomer-like spectrum). We can conclude that polymerisation has produced some longer conjugated segments. The HOMO-LUMO transitions in the monomer and dimer have quite different origins, as seen from the orbital surface plots of the respective transitions. The lowest weak transition for the monomer at about 520 nm is related to the trinitroamine moiety, which effectively disappears upon formation of the dimer.

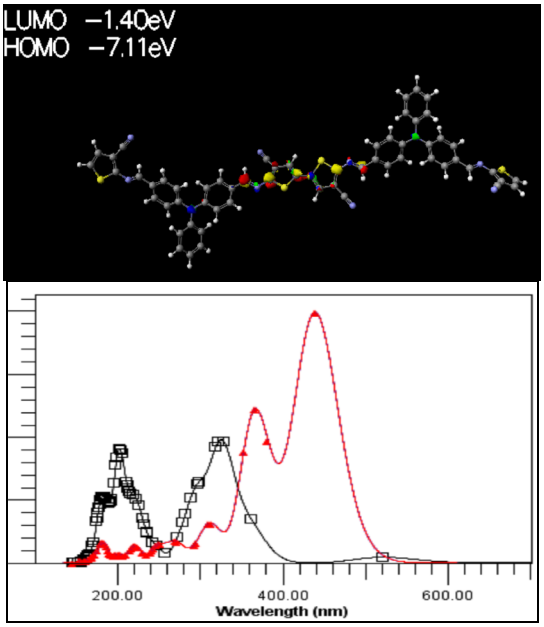

Figure 15. Geometry optimisation and predicted UV-vis spectrum of PTAZ4.

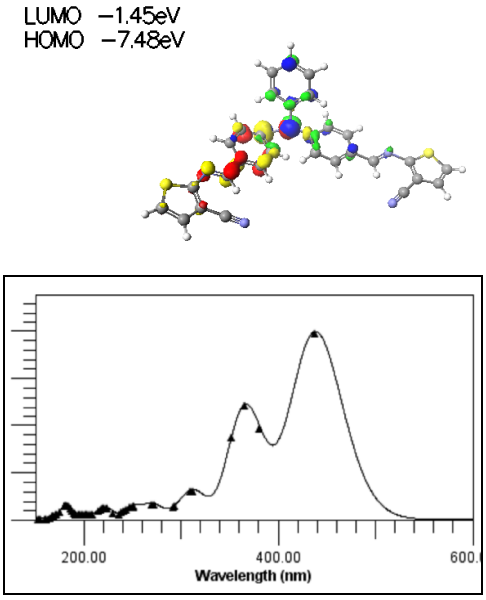

Figure 16. Geometry optimisation and calculated UV-visible spectrum of monomer THLC4.

5. CONCLUSIONS

New thiophene azomethine monomers have been successfully prepared and polymerised by oxidative polymerisation. The resulting polymers showed moderate molecular masses (calculated for their soluble fractions only). POM and DSC studies indicated that both the polymers and the monomers had liquid crystalline phases. The Tg values reflected the rigidity of the polymer backbones. Good films were obtained on spinning these polymers from their THF solutions onto quartz glass plates, probably due to the flexible side chains and main chain methylene spacers that improved their self-assembly properties. Cyclic voltammetry data indicated that the polymers had reversible oxidation behaviour. HOMO and LUMO energy levels ranged from -5.78 to -5.54 eV and -3.59 to -3.34 eV respectively. The electrochemical bandgaps were in the range 1.95-2.43 eV, and were in good agreement with those calculated from the UV-vis spectra. In solvents with different polarities such as DMF, DMSO and THF, there was only slight solvent-polarity dependence of the absorption wavelength positions in these polymers. Based on the results of the fluorescence studies in liquid phase, the polymers exhibited solvatochromism; the emission maxima of the polymers were red-shifted as the polarity increased, particularly for PTAZ2 and PTAZ3. Both PTAZ3 and PTAZ4 showed a slight increase in the emission wavelength after complexation with lanthanide ions, and this was accompanied by an increase in the emission intensity for PTAZ3-PTAZ4. Complexation may have led to better organisation of the polymer chains, which could enhance the emission properties by increasing the backbone rigidity and reducing intersystem crossing to the triplet state. The CN groups played a vital role in the improvement of the optoelectronic properties of these polymers, by increasing the electron affinity and shifting the emission towards longer wavelength. The presence of electron-donating alkoxy groups together with CN groups on the same polymeric backbone induces strong permanent dipoles and increases the electron density in the chromophoric block, consequently bringing about a decrease of the energy of the excited state and red-shifted emission. Current-voltage graphs for prototype PLED devices showed relatively low turn-on voltages (between 6.20 V for PTAZ3 and 8.0 V for PTAZ4). The devices produced electroluminescent spectra similar to the PL spectra of the corresponding samples, indicating that the emission originated from the same singlet states S_1. Molecular modelling experiments were performed on the polymers and monomers in order to optimise the geometrical conformations, and there was good agreement between the theoretical predictions and the relevant experimental data.

ACKNOWLEDGMENTS

We would like to thank the Ministry of Higher Education and Scientific Research, Iraq, for partial funding to support this work. We thank Tikrit University Iraq and Kingston University London for their help and support to accomplish this work.

REFERENCES

1. Grigoras M. and Catanesca C., Imine oligomers and polymers. *J. Macromol. Sci. C Polym. Rev.* **C44** (2004) 133-73.
2. Iwan A. and Sek D. Processible polyazomethines and polyketanils: From aerospace to light emitting diodes and other advanced applications. *Prog. Polym. Sci.* **33** (2008) 289-345.
3. Iwan A., Sek D., Rannou P., Kasperczyk J., Janeczek H., Mazurak Z, *et al*. Synthesis, characterization and optoelectronic properties of oligo ketanils containing C=C double bond in the main chain. *Synth. Met.* **143** (2004) 331-9.
4. Giuseppone N. and Lehn, J.-M. Constitutional organic self- sensing in zinc II/poly imino fluorenes systems. *J. Amer. Chem. Soc.*, **126** (2004) 11448-11449.
5. Lehn J.-M. Dynamic molecules and supramolecular polymers. *Polym. Sci.* **30** (2005) 814-831.
6. Bourgeaux M., Perez Guarin S.A. and Skene W.G. *J. Mater. Chem.* **17** (2007) 972.
7. Dufresne S., Bold A. and Skene W.G. *J. Mater. Chem.* **20** (2010) 4861.

8. Bold A., Dufresne S. and Skene W.G. *J. Mater. Chem.* **20** (2010) 4820.
9. Dufresne S., Roche I.U., Kalski T. and Skene W.G. *J. Phys. Chem.* **114** (2010) 13106.
10. Dufresne S., Bourgeaux M. and Skene W.G. *J. Mater. Chem.* **17** (2007) 1166.
11. El-Shekeil A.G., Al-Khader Ma and Abu Baker A.O. Synthesis, characterization, and dc electric conductivity of some oligomer mixed metal complexes. *Synth. Met.* **14** (2004) 147-152.
12. Khalid M.A., El-Shekeil A.G. and Al Yusufy F.A. A study of a thienylene-phenylene polyazomethine and its copper complexes. *Eur. Polym. J.* **37** (2001) 1423-1431.
13. Valchos P., Mansoor B., Aldred M.P., O'Neill M. and Kelly S.M. Charge transport in crystalline organic semiconductors with liquid crystalline order. *Chem. Commun.* **23** (2005) 2921-3.
14. Niu H. Luop, Zhang M. *et al*. Multifunctional, photochromic, acidochromic, electrochromic molecular switch: novel aromatic poly(azomethine)s containing a triphenylamine group. Eur. Polym. J. **45** (2009) 3058-3071.
15. Pinto M.R., Hu B., Karasz F.E. and Akcelrud L. Emitting polymers containing cyano groups. Synthesis and photophysical properties of fully conjugated polymers obtained by Wittig reaction. *Polymer* **41** (2000) 8095-8102.
16. Chio M., Kim H. and Suh D. Changes of fluorescence color in novel poly(azomethine) by the acidity variation. *J. Appl. Polym. Sci*. **101** (2006) 1228-1233.
17. Sugimoto R., Takeda S., Gu H.B. and Yoshino K. Preparation of soluble polythiophene derivatives utilizing transition metal halides as catalysts and their property, *Chemistry Express* **1** (1986) 635–638.
18. Loredana V., Teofilia I. and Micrea G. New symmetrical conjugated thiophene-azomethines containing triphenylamine or carbazole units: synthesis, thermal and optoelectrochemical properties. *High Performance Polymers* **24** (2012) 717-729.
19. Sek D., Iwan A., Jarzabek B., Kaczmarczyk B., Kasperczyk J. and Mazurak Z. Hole transport triphenylamine-azomethine conjugated system: synthesis, optical photoluminescence and electrochemical properties. *Macromolecules* **41**(18) (2008) 6653-63.
20. Jerca V.V., Nicolescu F.A., Baran A., Anghel D.F., Vasilescu D.S. and Vuluga D.M. *React. Funct. Polym.* **70** (2010) 827-835.
21. Huang Y.P., Tsai S.H., Huang D.F., Tsai T.S., Chow T.J. *React. Funct. Polym*. **67** (2007) 986-998.
22. Gupta V.D., Padalkar V.S., Phatangare K.R., Patil V.S., Umape P.G. and Sekar N. *Dyes Pigm.*, **88** (2011) 378-384.
23. Hu Z.J., Sun P.P., Li L., Tain Y.P., Yang J.X, Wu J.Y., Zhou H.P., Tao L.M., Wang C.K., Li M., Cheng G.H., Tang H.H., Tao X.T. and Jiang M.H., *Chem. Phys.*, **335** (2009) 91-98.
24. Measuring the ideality factor. Website: http://pveducation.org/pvcdrom/characterisation/measurement-of-ideality-factor.
25. Allan D. and Michael C.Z. *Theoretical Chemistry Accounts*, **53** (1979) 21-54.